crystals

MDPI

Article

Investigation into the Characteristics of Double-Layer Transparent Conductive Oxide ITO/TNO Anti-Reflection Coating for Silicon Solar Cells

Yih-Shing Lee [1,*], Li-Yang Chuang [1,2], Cheng-Jia Tang [1], Zi-Zhu Yan [1], Bing-Shin Le [1] and Cheng-Chung Jaing [1]

1 Department of Semiconductor and Electro-Optical Technology, Minghsin University of Science and Technology, Hsin-Fong, Hsinchu 30401, Taiwan
2 Green Energy and Environment Research Laboratories, Industrial Technology Research Institute, Chutung, Hsinchu 31040, Taiwan
* Correspondence: yslee@must.edu.tw; Tel.: +886-3-559-3142 (ext. 3383)

Abstract: In this study, indium–tin oxide (ITO)/Nb-doping TiO_2 (TNO) double-layer transparent conductive oxide (TCO) films deposited using DC magnetron sputtering were used as a surface anti-reflection layer with an overall thickness of 100 nm for double-layer films. The simulated results showed that ITO and TNO thickness combinations of 90 nm/10 nm, 80 nm/20 nm, and 70 nm/30 nm had a higher transmittance and lower reflectance than others in the visible wavelength range. Compared to the single-layer ITO films, for ITO/TNO films deposited on the glass and silicon substrates with an optimum thickness of 80/20 nm, the reflectance was reduced by 5.06% and 4.63%, respectively, at the central wavelength of 550 nm and crystalline silicon photo response wavelength of 900 nm. Moreover, the near-infrared reflectance of the double-layer ITO/TNO with thickness combinations of 90 nm/10 nm, 80 nm/20 nm, and 70 nm/30 nm, when deposited on silicon substrates, was obviously improved by the graded refractive index lamination effect of air (1)/ITO (1.98)/TNO (2.41)/Si (3.9).

Keywords: double-layer transparent conductive oxide; near-infrared reflectance; graded refractive index

check for updates

Citation: Lee, Y.-S.; Chuang, L.-Y.; Tang, C.-J.; Yan, Z.-Z.; Le, B.-S.; Jaing, C.-C. Investigation into the Characteristics of Double-Layer Transparent Conductive Oxide ITO/TNO Anti-Reflection Coating for Silicon Solar Cells. *Crystals* **2023**, *13*, 80. https://doi.org/10.3390/cryst13010080

Academic Editor: Robert F. Klie

Received: 20 November 2022
Revised: 23 December 2022
Accepted: 29 December 2022
Published: 1 January 2023

1. Introduction

The development of transparent conducting oxides (TCOs) has led to the evolution of a variety of optoelectronic devices, such as flat panel displays (FPDs), touch panels, and Si-based solar cells [1,2]. In new devices, including organic light-emitting diodes (OLEDs), copper indium gallium diselenide (CIGS) solar cells, and GaN-based blue LEDs, TCOs have been key materials. At present, $In_{2\text{-}x}Sn_xO_3$ (indium-tin oxide (ITO)) is the most widely used TCO because of its excellent transparent conducting properties [3,4] and its ease of fabrication. However, there is still a strong demand for new TCOs. This is due to the industrial need for high-efficiency optoelectronic devices. The properties of TCO greatly improve device performance by adopting a TCO whose refractive index matches that of the substrate. Furthermore, appropriate TCOs with high transmittance in the infrared region improve the efficiency of solar cells and OLEDs. A new TCO, anatase $Ti_{1\text{-}x}Nb_xO_2$ (TNO) [5,6], has similar electrical and optical properties to ITO. TNO has properties that ITO does not possess, such as a high refractive index, high transmission in the infrared region, and high chemical stability in the reduction of the atmosphere. The recombination of electrons and optical losses of the transparent conducting oxide (TCO) is one of the most serious issues in solar cells. It can be achieved using a suitable anti-reflection layer and contact coverage. Double-layer antireflective coatings based on a combination of silicon nitride (SiN) and silicon oxide SiO_2 result in a reflectance of 0.044, based on an AM I.5 photon flux ranging from 300 to 1150 nm [7]. Turkoglu et al. [8] recently represented the optimization of Zinc Tin Oxide/Silver/Zinc Tin Oxide (ZTO/Ag/ZTO) multilayers and implemented them in thin film solar cells as transparent electrodes. An electrical and optical characterization of these multilayers revealed that reduced sheet resistance and improved optical transmittance can be acquired for solar cells by the optimization of thin film thicknesses and position of the Ag within the multilayer.

Literature reviews on the application of double layers of TCOs on solar cells as an anti-reflection coating will be described in this paragraph. Ngaffo et al. [9] reported that although the single-layer ITO film has high transmittance, the transmittance of the double-layer ITO/TiO_2 films using reactive pulsed laser ablation deposition (RPLAD) is higher than the single ITO films in the UV-visible region. They reported that the refractive index (n) dependence on λ for TiO_2 films, annealed at 300 and 500 °C for TiO_2 films deposited at 400 °C, increased with the post-annealing temperature. The n for TiO_2 film annealed at 500 °C is close to that of the anatase phase. In a study of double-layer ITO/TiO_2 films, TiO_2 film was deposited on ITO film, revealing that a low IR transmittance leads to high IR reflectance, which is a desirable feature in window layer coatings, especially for applications in energy-efficient windows for solar cells [9,10]. Mardare et al. [11] reported that TiO_2/ITO films have been deposited onto glass in order to obtain visible-transmitting but solar-heat-reflecting coatings. TiO_2 doping with Ce, Nb, and Fe on ITO films achieves a higher transmittance in the visible range and a combined effect of dopants and substrate determined an increase in the reflectance and a decrease in the transmittance in the near-infrared (NIR) range. The effect is that the NIR optical transmittance of the ensemble TiO_2/ITO films can be modified. Noh et al. reported that Nb-doped TiO2 (TNO) layers deposited on conventional ITO substrates using pulsed laser deposition (PLD) enhanced the optical-to-electrical conversion efficiency of the dye-sensitized solar cells (DSSCs) by as much as 17% compared to that of bare ITO-based DSSCs. The electrical properties and *J-V* characteristics of the multilayered TNO/ITO films showed that the improved cell performance was due to the electrons passing through the interface between TNO and ITO using the tunneling effect that resulted from the formation of an ohmic contact with ITO [12]. However, TNO/ITO substrates exhibit lower transmittances at wavelengths longer than 550 nm compared to the bare-ITO substrate, which leads to a decrease in the effective number of incident photons. In general, the front TCO layer is a source of significant optical and electrical losses in silicon heterojunction solar cells because of the trade-off between free-carrier absorption and sheet resistance. Barraud et al. [13] reported that sputtered hydrogen-doped indium oxide (IO:H)/ITO bilayers with a thickness of 110 nm had low contact resistance, sheet resistance, and free-carrier absorption, outperforming IO:H-only or ITO-only layers in solar cells. Feldmann et al. [14] applied ITO/AZO double-layer TCO films with a thickness combination of 55/20 nm to heterojunction crystalline solar cells as an anti-reflection layer on the surface. The reflectance can be decreased by using such multiple layers with high and low refractive index values; it was concluded that the double-layer TCO film is suitable for use in a crystalline solar cell. However, the resistivity of AZO films increased with a further increase in the substrate temperature to 350 °C as a result of the decrease in carrier concentration and mobility [15]. However, few studies focusing on the effects that double-layer lamination of ITO/TNO TCOs with different thickness combinations on the optical and electric characteristics have been reported. In this work, a chemically stable and non-toxic material TNO with a wide band gap and higher refractive index was chosen to replace AZO films as the anti-reflection layers of the silicon solar cells using ITO and TNO double-layer TCOs with low and high refractive indices. Compared to the single-layer ITO films, in ITO/TNO films with an optimum thickness of 80/20 nm deposited on the glass and silicon substrates, the reflectance is clearly reduced as a result of the graded refractive index lamination effect. At first, the experimental conditions of the single-layer TNO and ITO films deposited on glass substrates were determined to optimize optoelectronic characteristics of the TCO films. Then, to achieve the graded refractive index lamination effect of air (1)/ITO (1.98)/TNO (2.41)/glass (1.52), optical parameters were used for a Macleod optical simulation of double-layer lamination with various film thicknesses, with the overall thickness of double-layer films being 100 nm. Finally, double layers of ITO and TNO films with the mentioned thickness combination were deposited on the respective glass and silicon substrates to achieve the optimum optical and electric characteristics. The experimental results indicate that the combination of double-layer ITO/TNO thickness and 80/20 nm provides sufficient lateral conductivity and reduces the front surface reflection on the silicon substrate.

2. Materials and Methods

First of all, TNO films were deposited on Eagle XG glass substrates at room temperature using a nominal composition of $Ti_{0.94}Nb_{0.06}O_2$ (purity, 99.99%) ceramic target with a 3 in. diameter. TNO films were prepared using a direct-current (dc) magnetron sputtering system (LJ-UHV LJ-303CL) at a fixed deposition power of 175 W. The background pressure in the sputtering system was 4×10^{-4} Pa and the process pressure was 0.67 Pa. The flow rate of the Ar and O_2 gas mixture was fixed at 40 sccm, in which the oxygen (O_2) flow ratios varied from 0.1% to 0.3% to find the optimum optoelectronic properties of TNO films. After TNO deposition, the samples were annealed for 1 h using a horizontal annealing furnace tube at a vacuum pressure of 0.4 Pa at temperatures varying from 400 °C to 600 °C. Afterwards, ITO films were deposited on SCHOTT B270 glass substrates at room temperature using a nominal composition of (Sn_2O_3: In_2O_3 = 10 wt%: 90 wt%, target purity: 99.99%) ceramic target with an 8 in. diameter. ITO films were deposited by dc magnetron sputtering system (GENCOA SW/PP300) at room temperature, in which the deposition power density was fixed at 0.54 W/cm^2. The background pressure in the sputtering system was 4×10^{-4} Pa and process pressure was 0.267 Pa. The flow rate of Ar was fixed at 20 sccm, and O_2 flow rates varied from 0 to 0.6 sccm to find the optimum transmittance and resistivity of ITO films. In order to improve the transmittance and electrical conductivity of ITO films, the hydrogen (H_2) flow rate was added, ranging from 0 to 0.3 sccm. The crystallinity of TNO films was also investigated using grazing incidence X-ray diffraction (GIXRD) (PANalytical X'Pert Pro) analysis with a Ni-filtered Cu Kα (λ = 1.5418 Å) source at a glancing incident angle of 1°. The scanning range was between 2θ = 20° and 80°. The film thickness, refractive index, and extinction coefficient were examined and fitted by using a spectroscopic ellipsometer (SE) (M-2000U) and CompleteEASE software (J. A. Woollam Co., Inc., Lincoln County, NE, USA), respectively. The measurement was carried out in the wavelength range of 370–1000 nm at the incident angles of 50°, 60°, and 70°. The optical transmittance (T%) and reflectance (R%) spectra of these films were scanned in the wavelength (λ) range of 340–1200 nm using a UV–visible spectrophotometer (LAMBDA UV Lambda 900). The film resistivity was performed by the four-point probe method using 3S, MFP series (Swin). Optical coating design and simulations with the Essential Macleod (Thin Film Center Inc., Tucson, AZ, USA) were carried out using the refractive indices (n) and extinction coefficients (k) of the mentioned ITO and TNO experiments after optimizing optoelectronic properties. The trends of transmittance and reflectance spectra in the wavelengths (λ) range of 350–1000 nm for double-layer ITO/TNO thickness combinations of 100/0, 90/10, 80/20, 70/30 and 60/40 nm were simulated. In addition, the optical designed layers from the top surface were a medium, ITO, TNO, and substrate in sequence, and the refractive indices of the air medium and the glass substrate are set as 1.0 and 1.52, respectively. Figure 1 shows the schematic figure of double-layer ITO/TNO on the glass substrate and the direction of light used in this study. Finally, the aforementioned thickness combination of double-layer ITO/TNO films was deposited on the respective glass and silicon substrates, and ITO films were deposited on the TNO film by controlling the overall thickness of 100 nm. The optical transmittance (T%), reflectance (R%) spectra, and film resistivity of double-layer ITO/TNO films were measured to find the optimum thickness combination. The methods of measuring and fitting the film thickness of the ITO/TNO bilayer film are as follows.

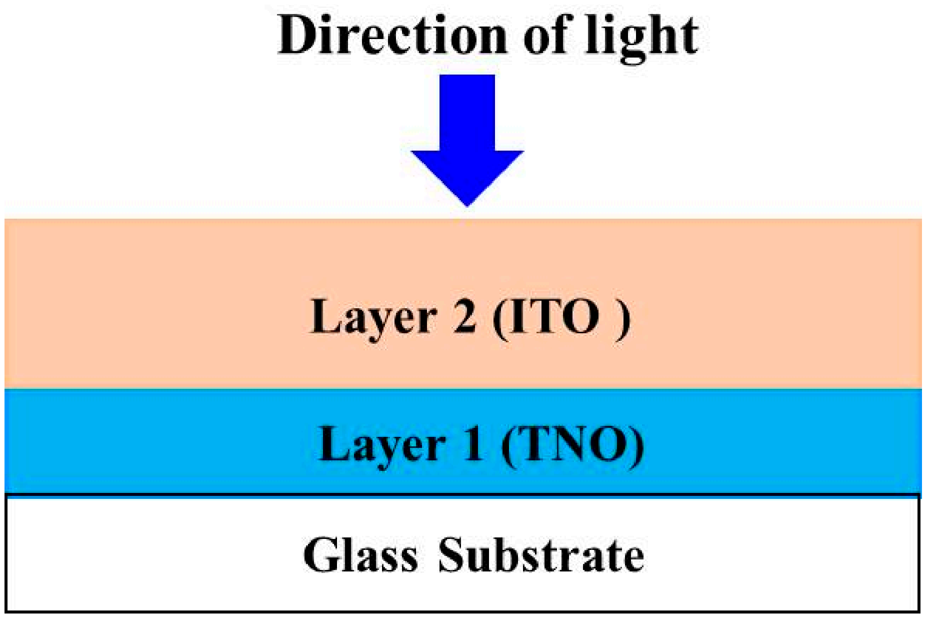

Figure 1. Schematic diagram of double-layer indium-tin oxide (ITO)/ $Ti_{1-x}Nb_xO_2$ (TNO) on the glass substrate and the direction of light.

First, measure the thickness data of the first layer of the TNO film, and use the effective medium approximation (EMA) model with Cauchy equation to fit the film thickness, refractive index, and extinction coefficient. The formula is as follows [16,17]:

$$n(\lambda) = A + B/\lambda^2 + C/\lambda^4 \tag{1}$$

where n is the refractive index, λ is the wavelength, and A, B, and C are coefficients that can be determined for a material by fitting the equation to measured refractive indices at known wavelengths.

$$k(\lambda) = \alpha \cdot e^{\beta\ \{12{,}400\ (1/\lambda - 1/\gamma)\ \}} \tag{2}$$

where α, β, and γ are coefficients that can be determined for a material by fitting the equation to the measured extinction coefficient at known wavelengths. Then, the substrate data and TNO film data were fixed to use these values to find the fitting parameters of the second layer of the ITO film (the n value varies slightly, between about 1.8 and 2.1).

3. Results and Discussion

3.1. TNO Films by Changing O_2 Ratios and Annealing Temperature

Figure 2a shows the XRD patterns of the TNO films deposited at various powers with an O_2 ratio of 0.1% and annealed at a temperature of 600 °C. Figure 2b,c show the XRD patterns of the TNO films deposited at a power of 175 W with the O_2 ratio of 0.1% and 0.2%, respectively, and annealed at various temperatures. As shown in Figure 1, all films presented the mixed crystalline phases between anatase TiO_2 (JCPDS file no. 21-1272) and Nb_2O_5 (JCPDS file no. 43-1042). All the samples exhibit A(1 0 1) as their preferred orientation. The A(1 0 1) and A(2 0 0) dominated peaks, which confirm the TiO_2 structure can show the crystallite quality of samples [18,19]. Previous results [20] showed that when the deposition power increased, the average transmittance ($T_{avg.}$) in the visible light wavelength range of 400–800 nm and the average refractive index ($n_{avg.}$) increased. Moreover, the resistivity of TNO films decreased as the deposition power and annealing temperature increased, which could be ascribed to the grain growth of the anatase TiO_2 crystalline phase measured from XRD spectra of TNO thin films, as shown in Figure 2a,b. Fallah et al. [19] confirmed that oxygen in the annealing process plays an important role in the optical transparency and electrical conductivity of TNO thin films, so gradual vacuum annealing could offer TNO thin films a chance to obtain better nucleation and more desired crystallites in the anatase TiO_2 crystalline phase. The optical and resistivity properties of TNO films by changing O_2 ratios and annealing temperatures at a fixed deposition power of 175 W are summarized in Table 1. The T_{avg} of TNO films deposited at an O_2 ratio of 0.1% decreased from 78.2% to 72.3%, and the resistivity decreased from 4.4×10^3 Ω·cm to 3.4×10^{-3} Ω·cm as the annealing temperature increased. Neither the $T_{avg.}$ nor resistivity of TNO films deposited at an O_2 ratio of 0.2% significantly decrease as the annealing temperature increases. The lowest resistivity of TNO films is 1.8×10^{-3} Ω·cm at an annealing temperature of 400 °C. This is ascribed to the significant grain growth of the anatase TiO_2 crystalline phase measured using the XRD spectra of TNO thin films deposited at the O_2 ratio of 0.2% and annealing at 400 °C, as shown in Figure 2c. Although both the average transmittance and refractive index of TNO films deposited at the O_2 ratio of 0.3% increased, the resistivity rose between -2.2×10^{-2} and 4.5 Ω·cm at different annealing temperatures. Figure 3a shows the transmittance and reflectance spectra for TNO films deposited at an O_2 ratio of 0.2% as a function of wavelength with various annealing temperatures. Figure 3b,c show the fitted refractive index (n) and extinction coefficient (k) of TNO films deposited at an O_2 ratio of 0.2% with various annealing temperatures as a function of wavelength, respectively. The refractive index and extinction coefficient of the TNO films maintained a fixed value with various annealing temperatures, except the extinction coefficient of the TNO films annealed at 600 °C slightly increased.

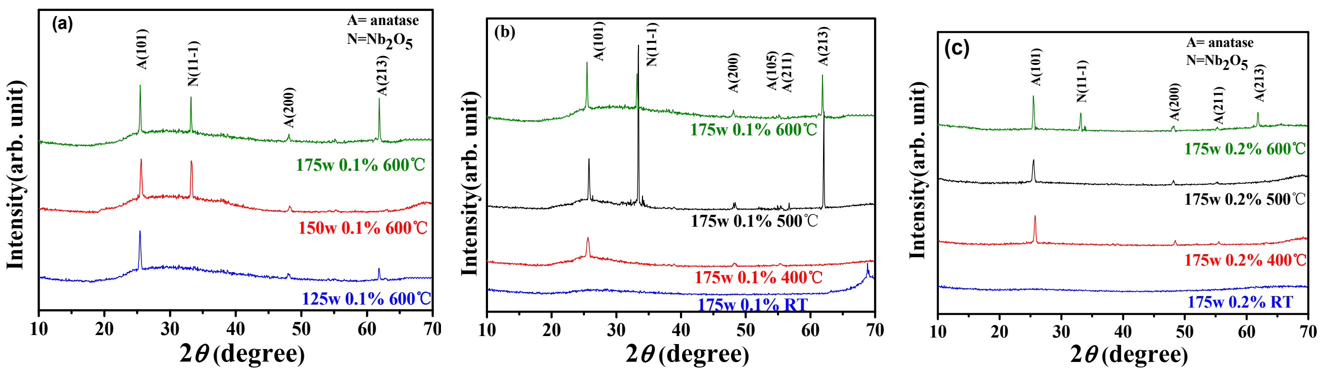

Figure 2. XRD patterns of TNO films (**a**) deposited at various powers with an O_2 ratio of 0.1% and annealed at a temperature of 600 °C, and deposited at a power of 175 W with O_2 ratio at (**b**) 0.1%, (**c**) 0.2% and annealed at various temperatures. RT is the samples as deposited at the room temperature.

Table 1. Optical and resistivity properties of TNO films by changing O_2 ratios and annealing temperatures at a fixed deposition power of 175 W.

f_{O2} (%)	Annealing Temperature (°C)	$T_{avg,}$ (%) [1]	Refractive Index, $n_{avg.}$ [1]	Extinction Coefficient, $k_{avg.}$ [1]	Resistivity (Ω·cm)
0.1	400	78.2	2.41	0.016	4.4×10^3
0.1	500	75	2.43	0.029	1.1×10^{-1}
0.1	600	72.3	2.39	0.041	3.4×10^{-3}
0.2	400	76.9	2.41	0.0005	1.8×10^{-3}
0.2	500	74.1	2.41	0.0005	6.4×10^{-3}
0.2	600	74.9	2.42	0.0009	2.3×10^{-3}
0.3	400	79.2	2.48	0.007	4.5×10^0
0.3	500	77.5	2.49	0.002	8.2×10^{-1}
0.3	600	76.1	2.45	0.0001	2.2×10^{-2}

[1] $T_{avg.}$, n_{avg}, and k_{avg} are averaged over the visible wavelength range of 400–800 nm.

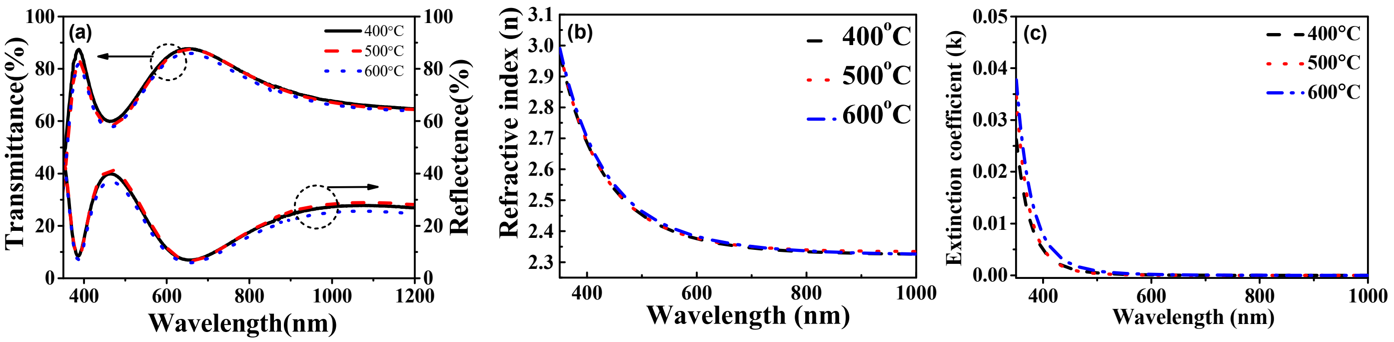

Figure 3. (**a**) Transmittance and reflection spectra, (**b**) the fitted refractive index (n) and (**c**) extinction coefficient (k) of TNO films deposited at O_2 ratio of 0.2% with various annealing temperatures as a function of wavelength.

3.2. ITO Films Deposited by Changing O_2 Flow Rates and at Various H_2 Flows

The optical and resistivity properties of ITO films by changing O_2 flow rates are summarized in Table 2. As the oxygen flow increased, the T_{avg} of ITO films increased, and the deposition rate and resistivity decreased. n_{avg} does not change much when the oxygen flow is between 0 and 0.4 sccm, but n_{avg}. tends to increase when the O_2 flow rate is between 0.5 and 0.6 sccm. Table 2 shows that the O_2 flow rates with the best transmittance and electrical conductivity are 0.3 and 0.4 sccm. Figure 4a shows the transmittance and reflectance spectra of ITO films deposited at various hydrogen flows at an oxygen flow of 0.3 sccm as a function of wavelength. The $T_{avg.}$ slightly increased in ITO films, to the saturation value of 81.6%, and the resistivity of ITO films gradually decreased to 3×10^{-4} Ω·cm at a hydrogen flow of 0.3 sccm. Zhang et al. [21] developed low-temperature deposition of thin films of ITO prepared by the radio frequency magnetron sputtering method by introducing H_2 into the sputtering gas mixture during the film preparation. The presence of H_2 gas in the sputtering processes was also shown to increase the number of charge carriers in the ITO films. At optimal deposition conditions, thin films of ITO were achieved, with a resistivity of 4.66×10^{-4} Ω·cm and an optical transmission of over 86% in the visible spectrum range. The relatively low film resistivity was attributed to the increased oxygen deficiency. Figure 4b,c show the fitted refractive index (n) and extinction coefficient (k) of ITO films deposited at various hydrogen flows at an oxygen flow of 0.3 sccm as a function of wavelength, respectively. The refractive index of the ITO films deposited at various hydrogen flows maintained a fixed value. The extinction coefficient of the ITO films gradually decreased as the hydrogen flows increased.

Table 2. Optical and resistivity properties of ITO films by changing O_2 flow rates.

O_2 (sccm)	Deposition Rate (nm/s)	$T_{avg.}$(%) [1]	Refractive Index, n_{avg} [1]	Extinction Coefficient, k_{avg} [1]	Resistivity (Ω·cm)
0	0.72	72.1	2.03	0.07	1.1×10^{-3}
0.1	0.78	75.2	2.0	0.03	5.5×10^{-4}
0.3	0.76	78.3	2.01	0.03	4.6×10^{-4}
0.4	0.74	77.5	2.02	0.01	4.5×10^{-4}
0.5	0.72	75.6	2.05	0.02	5.3×10^{-4}
0.6	0.69	75.3	2.08	0.02	1.1×10^{-3}

[1] $T_{avg.}$, n_{avg}, and k_{avg} are averaged over the visible wavelength range of 400–800 nm.

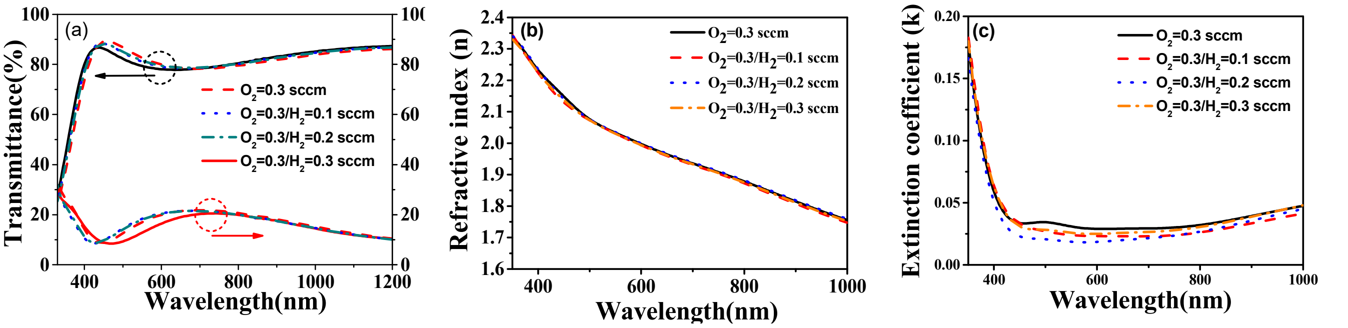

Figure 4. (**a**) Transmittance and reflection spectra, (**b**) the fitted refractive index (n) and (**c**) extinction coefficient (k) of ITO films deposited at various hydrogen flows at an oxygen flow of 0.3 sccm as a function of wavelength.

3.3. Simulated and Experimental Results of Double-Layer ITO/TNO with Different Thickness Combination

Using refractive indices (n) and extinction coefficients (k) of ITO and TNO films with optimized optoelectronic properties, the optical design and simulation of the double-layer anti-reflection films were carried out. Optimum optical results of the single-layer TNO and ITO films and experimental conditions with a thickness of 100 nm deposited on glass substrate are shown in Table 3. The average transmittance ($T_{avg.}$(%)), average reflectance ($R_{avg.}$(%)), refractive index ($n_{avg.}$), and extinction coefficient ($k_{avg.}$) were calculated in the wavelength range of 400–800 nm. To achieve the graded refractive index lamination effect of Air (1)/ITO (1.98)/TNO (2.41)/Glass (1.52), the parameters listed in Table 3 were used for a Macleod optical simulation of double-layer lamination with varying film thicknesses. Double-layer ITO/TNO was adopted for the anti-reflection layers in this study. The overall thickness for optical simulation was 100 nm. Figure 5a shows the simulated transmittance and reflectance spectra of double-layer ITO/TNO with different thickness combinations on the glass substrates as a function of wavelength. Double-layer ITO/TNO had a higher transmittance and a lower reflectance than the single-layer ITO in the visible wavelength range of 450–650 nm. Figure 5b shows the corresponding absorpance (A) spectra in the wavelength range of 350–1000 nm, calculated from the equation A = 1 − (T + R), in which T and R are the respective transmittance and reflectance, as shown in Figure 5a. Double-layer ITO/TNO had a lower absorptance than the single-layer ITO for all the simulated wavelengths. Figure 5c shows the corresponding simulated average transmittance, reflectance, and absorptance in the wavelength range of 400–800 nm. The results showed that ITO and TNO thickness combination with 90 nm/10 nm, 80 nm/20 nm, and 70 nm/30 nm achieved higher transmittance and lower reflectance than others in the visible wavelength range. Moreover, the average absorptance gradually decreased as the thickness of the TNO film increased, which is ascribed to the lower extinction coefficient of the TNO film. Double layers of ITO and TNO films used to experiment with the mentioned thickness combination will be conducted as follows.

Table 3. Optimum optical experimental result of the respective single-layer ITO and TNO.

Materials	$T_{avg.}$ (%)	$R_{avg.}$ (%)	Refractive Index, $n_{avg.}$	Extinction Coefficient, $k_{avg.}$
TNO (Ti:Nb = 94 at%:6 at%)	76.9	19.7	2.41	0.0005
ITO (Sn_2O_3:In_2O_3 = 10 wt%:90 wt%)	81.6	17.6	1.98	0.04

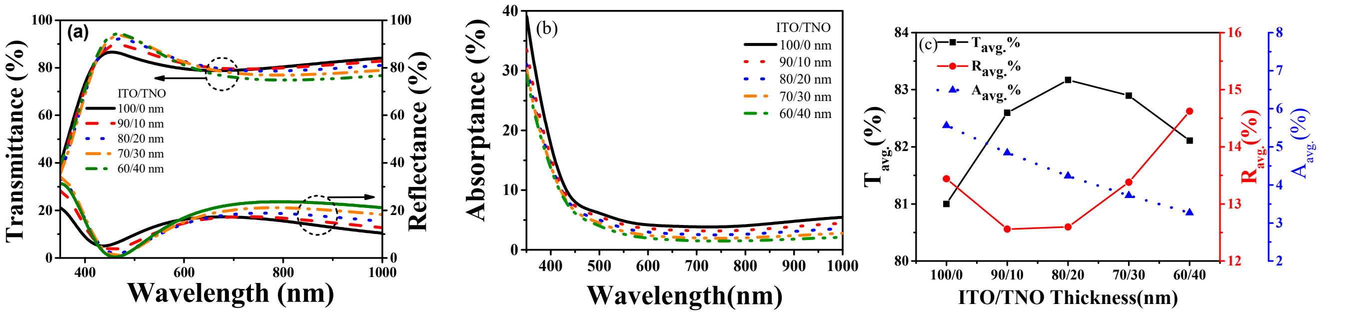

Figure 5. (**a**) Macleod simulated transmittance and reflectance spectra of double-layer ITO/TNO with different thickness combinations on the glass substrates as a function of wavelength, (**b**) corresponding absorptance spectra, and (**c**) corresponding simulated average transmittance, reflectance, and absorptance in the wavelength range of 400–800 nm.

Figure 6a shows the experimental transmittance and reflectance spectra of double-layer ITO/TNO with different thickness combinations on glass substrates as a function of wavelength. The experimental results show that double-layer ITO/TNO had a higher transmittance and lower reflectance than the single-layer ITO in the visible wavelength range of 450–650 nm, except for 60/40 nm double-layer stacks. The results show that the double layer with 80 nm ITO and 20 nm TNO had the highest transmittance and the lowest reflectance, with the same tendency as the simulated result, as shown in Figure 6c. According to the equation of the optical thickness of $nd = \frac{1}{4}\lambda_0$ (where n is the refractive index, d is the film thickness, λ_0 is the central wavelength 550 nm), an ITO thickness of around 70–80 nm revealed the lowest reflectance from the double-layer combination. Figure 6b shows the corresponding absorptance (A) in the wavelength range of 350–1200 nm, calculated from the equation A = 1 − (T + R). In addition, the absorptance in the wavelength of 350–400 nm increased abruptly, by 10%, and was below 10% in the wavelength of 400–1200 nm. However, ITO/TNO (60/40 nm) had the highest absorptance of 5% in the wavelength range of 400–800 nm, as shown in Figure 5c. According to the equation of the optical thickness of $nd = \frac{1}{4}\lambda_0$, $n^2 = n_{Si}n_0$ where n is the refractive index, d is the film thickness, λ_0 is the central wavelength 550 nm, $n_0 = 1$, $n_{Si} = 3.9$, the ITO thickness at around 70–80 nm reveals the lowest reflectance when the film refractive index is 1.97. From the double-layer ITO/TNO thickness combination of 60/40 nm, the R% abruptly increased (2.95%) and T% largely decreased (~5.9%); as a result, the absorption abruptly increased (~2.95%) compared to the double-layer ITO/TNO thickness combination of 70/30 nm, as shown in Figure 6c. Figure 7 shows trends in experimental reflectance (R%) at the center wavelength of 550 nm and resistivity for double-layer ITO/TNO with different thickness combinations deposited on the glass substrates. The resistivity of double-layer ITO/TNO films gradually increased with an increase in the thickness of TNO films. Compared with the ITO monolayer deposited on the glass substrate, the reflectance at the center wavelength of 550 nm is 16.1%, and the resistivity is 3.4×10^{-4} Ω·cm. The double-layer ITO/TNO thickness combination at 80/20 nm had the lowest reflectance of 11.06% and a good resistivity of 4.85×10^{-4} Ω·cm.

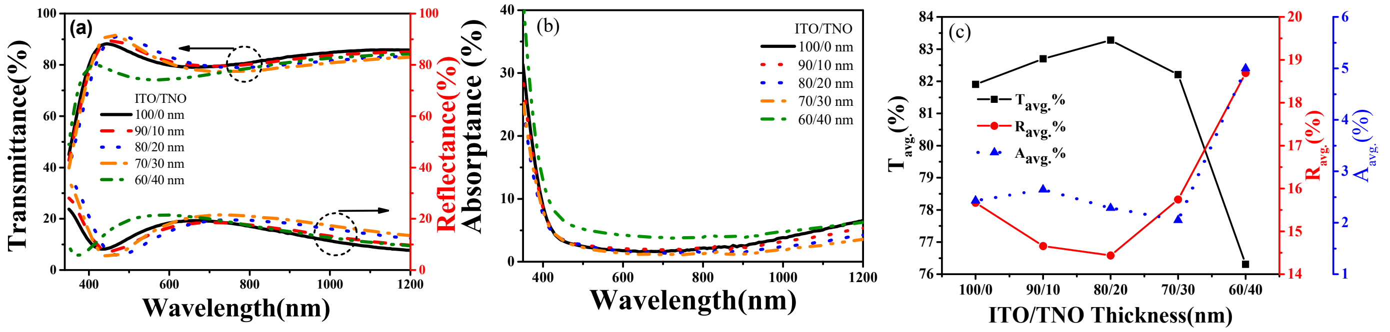

Figure 6. (**a**) Experimental transmittance and reflectance spectra of double-layer ITO/TNO with different thickness combinations on the glass substrates as a function of wavelength; (**b**) corresponding absorptance spectra; (**c**) corresponding average transmittance, reflectance, and absorptance in the wavelength range of 400–800 nm.

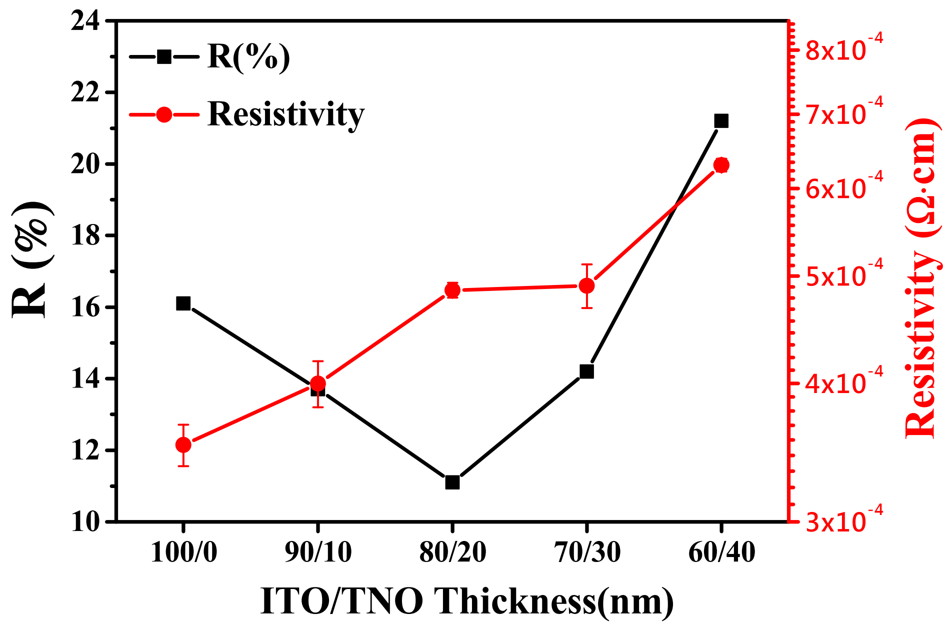

Figure 7. Trends of reflectance at the center wavelength of 550 nm and resistivity for double-layer ITO/TNO with different thickness combinations deposited on the glass substrates.

To compare graded refractive index lamination effects of Air (1)/ITO (1.98)/TNO (2.41) on the glass substrate, a double-layer ITO/TNO with different thickness combinations was deposited on silicon substrates. Figure 8a shows the reflectance spectra of double-layer ITO/TNO with different thickness combinations, deposited on silicon substrates as a function of the wavelength. The results indicated that, in the visible wavelength ranges of the 400~800 nm band, the reflectance on the silicon substrate is significantly greater than those on the glass substrate, whereas the reflectance on the silicon substrate in the near-infrared region decreased. The respective R% at the central wavelength of 550 nm and at a crystalline silicon photo response wavelength of 900 nm for double-layer ITO/TNO with different thickness combinations, deposited on glass and silicon substrates, are summarized in Table 4. The reflectance of the double-layer ITO/TNO thickness combination with 90 nm/10 nm, 80 nm/20 nm, and 70 nm/30 nm, deposited on the silicon substrate, decreased by less than 1% at a wavelength of 900 nm, and these three thickness combinations showed a better anti-reflection effect in the near-infrared region. However, at the central wavelength of 550 nm, the lowest reflectance on silicon substrates was 17.40% when the thickness combination of ITO and TNO films was 70 nm and 30 nm, respectively, and the lowest reflectance on glass substrates was 11.06% when the thickness combination of ITO and TNO films was 80 nm and 20 nm, respectively, as shown in Table 4. The best photon absorption wavelength for a single crystalline silicon solar cell was 900 nm for 300 nm−1200 nm [22]. Compared to the single-layer ITO films, with the double-layer ITO/TNO thickness combination with 80/20 nm, the reflectance on the glass substrate is reduced by 5.06% at a central wavelength of 550 nm and reflectance on the silicon substrate is reduced by 4.63% at a crystalline silicon photo response wavelength of 900 nm. Figure 8b depicts a schematic diagram of double-layer ITO/TNO on the silicon substrate. According to differences in the refractive index between Si (n = 3.9) and glass (n = 1.52), the near-infrared reflectance of double-layer ITO/TNO thickness combination with 80 nm/20 nm and 70 nm/30 nm, deposited on silicon substrates, decreased by less than 1% in Table 4, which is ascribed to the graded refractive index lamination effect of air (1)/ITO (1.98)/TNO (2.41)/Si (3.9).

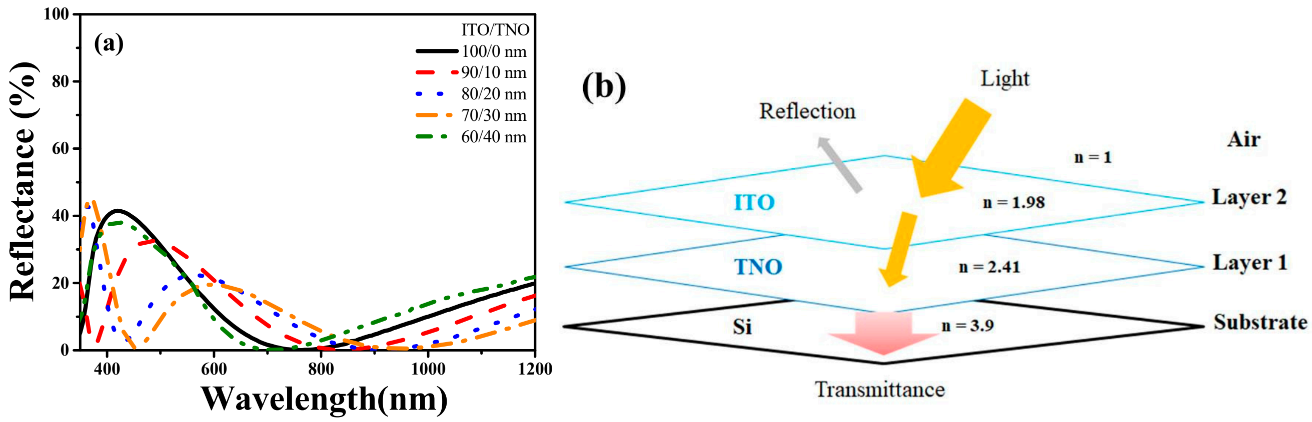

Figure 8. (**a**). Reflectance spectra of double-layer ITO/TNO with different thickness combinations deposited on the silicon substrate as a function of wavelengths. (**b**) Schematic diagram of double-layer ITO/TNO on the silicon substrate explains the graded refractive index lamination effect.

Table 4. Respective R% at the central wavelength of 550 nm and at crystalline silicon photo response wavelength of 900 nm for double-layer ITO/TNO with different thickness combinations deposited on glass and silicon substrates.

ITO/TNO Thickness (nm)	R% on Glass at 550 nm	R% on Si at 550 nm	R% on Glass at 900 nm	R% on Si at 900 nm
100/0	16.12	21.30	14.30	4.70
90/10	13.72	27.65	15.63	1.01
80/20	11.06	22.13	18.27	0.07
70/30	14.19	17.40	19.57	0.95
60/40	21.23	21.36	14.99	8.36

4. Conclusions

In this study, the optical and resistivity properties of the TNO films were optimized by changing O_2 ratios and annealing temperatures at a fixed dc power of 175 W, and the optimum optical and electric characteristics of the ITO films were prepared by the dc magnetron sputtering method by introducing oxygen and hydrogen into the sputtering gas mixture during the film preparation. To achieve the graded refractive index lamination effect of air (1)/ITO (1.98)/TNO (2.41)/glass (1.52), optical parameters were used for the Macleod optical simulation of double-layer lamination with varying film thicknesses; the overall thickness of double-layer films is 100 nm. Simulated results showed that ITO and TNO thickness combination with 90 nm/10 nm, 80 nm/20 nm, and 70 nm/30 nm had higher transmittance and lower reflectance than others in the visible wavelength range. Compared with the ITO monolayer deposited on the glass substrate, the reflectance at the center wavelength of 550 nm is 16.1%, and the resistivity is 3.4×10^{-4} Ω·cm. The double-layer ITO/TNO thickness combination at 80/20 nm has the lowest reflectance of 11.06% and has a good resistivity of 4.85×10^{-4} Ω·cm. Compared to the single-layer ITO films, with a double-layer ITO/TNO thickness combination with 80/20 nm, the reflectance on the glass substrate is reduced by 5.06% at a central wavelength of 550 nm and the reflectance on the silicon substrate is reduced by 4.63% at a crystalline silicon photo response wavelength of 900 nm. The near-infrared reflectance of double-layer ITO/TNO thickness combination with 90 nm/10 nm, 80 nm/20 nm, and 70 nm/30 nm deposited on silicon substrates was improved by the graded refractive index lamination effect of Air (1)/ITO (1.98)/TNO (2.41)/Si (3.9). The experimental results indicate that the double-layer ITO/TNO thickness combined with 80/20 nm provides sufficient lateral conductivity and obviously reduces the front surface reflection for silicon solar cells.

Author Contributions: Conceptualization, Y.-S.L. and L.-Y.C.; methodology, L.-Y.C. and C.-J.T.; software, L.-Y.C., C.-J.T. and C.-C.J.; validation, C.-J.T. and B.-S.L.; formal analysis, L.-Y.C.; investigation, Z.-Z.Y.; resources, L.-Y.C. and C.-C.J.; data curation, Z.-Z.Y.; writing—original draft preparation, Y.-S.L. and L.-Y.C.; writing—review and editing, Y.-S.L.; L.-Y.C., C.-J.T., Z.-Z.Y., B.-S.L. and C.-C.J. All authors have read and agreed to the published version of the manuscript.

Funding: This research were funded by the Ministry of Science Technology Project (MOST 110-2637-E-159-004) and the National Science and Technology Council Project (NSTC 112-NU -E-159-001 –NU).

Acknowledgments: The authors would like to thank Chorng-Jye Huang, the technical director of the photovoltaic technology department, as well as the green energy and environment research laboratories for supplying the dc magnetron sputtering system.

Conflicts of Interest: The authors declare no conflict of interest.

References

1. Ginley, D.S.; Bright, C. Transparent Conducting Oxides. *Mater. Res. Bull.* **2000**, *25*, 15–18.
2. Hartnagel, H.-L.; Dawar, A.-L.; Jain, A.-K.; Jagadish, C. *Semiconducting Transparent Thin Films*; Institute of Physics: Bristol, UK, 1995.
3. Pan, C.A.; Ma, T.P. High-quality transparent conductive indium oxide films prepared by thermal evaporation. *Appl. Phys. Lett.* **1980**, *37*, 163–165.
4. Hamberg, I.; Granqvist, C.G. Evaporated Sn-doped In_2O_3 films: Basic optical properties and applications to energy-efficient windows. *J. Appl. Phys.* **1986**, *60*, R123–R159. [CrossRef]
5. Furubayashi, Y.; Hitosugi, T.; Yamamoto, Y.; Inaba, K.; Kinoda, G.; Hirose, Y.; Shimada, T.; Hasegawa, T. A transparent metal: Nb-doped anatase TiO_2. *Appl. Phys. Lett.* **2005**, *86*, 252101. [CrossRef]
6. Hitosugi, T.; Furubayashi, Y.; Ueda, A.; Itabashi, K.; Inaba, K.; Hirose, Y.; Kinoda, G.; Yamamoto, Y.; Shimada, T.; Hasegawa, T. Ta-doped Anatase TiO_2 Epitaxial Film as Transparent Conducting Oxide. *Jpn. J. Appl. Phys.* **2005**, *44*, L1063–L1065. [CrossRef]
7. Wright, D.N.; Marstein, E.S.; Holt, A. Double layer anti-reflective coatings for silicon solar cells. In Proceedings of the Thirty-first IEEE Photovoltaic Specialists Conference, Lake Buena Vista, FL, USA, 3–7 January 2005.
8. Turkoglu, F.; Koseoglu, H.; Ekmekcioglu, M.; Cantas, A.; Ozdemir, M.; Aygun, G.; Ozyuzer, L. Development of ZTO/Ag/ZTO transparent electrodes for thin film solar cells. *J. Mater. Sci. Mater. Electron.* **2022**, *33*, 10955–10964. [CrossRef]
9. Fotsa-Ngaffo, F.; Caricato, A.P.; Romano, F. Optical properties of ITO/TiO_2 single and double layer thin films deposited by RPLAD. *Appl. Surf. Sci.* **2009**, *255*, 9684–9687. [CrossRef]
10. Gordon, R.G. Transparent Conducting Oxides. In *MRS Bulletin*; Cambridge University Press: Cambridge, UK, 2000; Volume 25, pp. 52–57.
11. Mardare, D.; Apostol, E. TiO_2 thin films doped by Ce, Nb, Fe, deposited onto ITO/glass substrates. *J. Optoelectron. Adv. Mater.* **2006**, *8*, 914–916.
12. Noh, J.H.; Lee, S.; Kim, J.Y.; Lee, J.K.; Han, H.S.; Cho, C.M.; Cho, I.S.; Jung, H.S.; Hong, K.S. Functional multilayered transparent conducting oxide thin films for photovoltaic devices. *J. Phys. Chem. C* **2009**, *113*, 1083–1087. [CrossRef]
13. Barraud, L.; Holman, Z.C.; Badel, N.; Reiss, P.; Descoeudres, A.; Battaglia, C.; De Wolf, S.; Ballif, C. Hydrogen-dopedindiumoxide/indium tin oxide bilayers for high-efficiency silicon heterojunction solar cells. *Sol. Energy Mater. Sol. Cells* **2013**, *115*, 151–156. [CrossRef]
14. Feldmann, F.; Reichel, C.; Müller, R.; Hermle, M. The application of poly-Si/SiOx contacts as passivated top/rear contacts in Si solar cells. *Sol. Energy Mater. Sol. Cells* **2017**, *159*, 265–271. [CrossRef]
15. Zhang, Z.; Bao, C.; Yao, W.; Ma, S.; Zhang, L.; Hou, S. Influence of deposition temperature on the crystallinity of Al-doped ZnO thin films at glass substrates prepared by RF magnetron sputtering method. *Superlattices Microstruct.* **2011**, *49*, 644–653. [CrossRef]

16. Xie, H.; Wei, J.; Zhang, X. Characterisation of Sol-gel Thin Films by Spectroscopic Ellipsometry. *J. Phys. Conf. Ser.* **2006**, *28*, 95–99. [CrossRef]
17. J.A. Woollam Co., Inc. *Guide to Using WVASE*; J.A. Woollam Co., Inc.: Lincoln, NE, USA, 1999; Volume 32, p. 159.
18. Li, W.; Ni, C.; Lin, H.; Huang, C.; Shah, S.I. Size dependence of thermal stability of TiO2 nanoparticles. *J. Appl. Phys.* **2004**, *96*, 6663–6668. [CrossRef]
19. Fallaha, M.; Zamani-Meymian, M.-R.; Rabbani, M. Influence of two gradual steps of vacuum annealing on structural and opto-electronic characteristics of Nb-doped TiO_2 transparent conducting oxide. *Superlattices Microstruct.* **2018**, *123*, 242–250. [CrossRef]
20. Lee, Y.-S.; Tang, C.-J.; Zhang, Y.-S. Effects of deposition power and annealing temperature of $Ti_{1\text{-}x}Nb_xO_2$ transparent conductive films. In *Optics & Photonics Taiwan International Conference (OPTIC)*; National Chung Hsing University: Taichung, Taiwan, 2019.
21. Zhang, K.; Zhu, F.; Huan, C.H.A.; Wee, A.T.S. Indium tin oxide films prepared by radio frequency magnetron sputtering method at a low processing temperature. *Thin Solid Film* **2000**, *376*, 255–263. [CrossRef]
22. Sze, S.M. *Semiconductor Device Physics and Technology*; John Wiley & Sons: New York, NY, USA, 1981.